PERGAMON

Chemical Engineering Science 54 (1999) 5761–5775

Chemical Engineering Science

Experimental investigation of Taylor bubble acceleration mechanism in slug flow

E. T. Tudose, M. Kawaji*

Department of Chemical Engineering and Applied Chemistry, University of Toronto, Toronto, Ont., Canada M5S 3E5

Abstract

Measurements of the total drag force on a stationary, solid model of a Taylor bubble placed in a downward flowing liquid stream in a vertical tube have been performed and analyzed using a one-dimensional flow model, in order to study the mechanisms responsible for acceleration of a Taylor bubble in the wake region of a preceding Taylor bubble in gas–liquid slug flow. Variations in the drag force with the solid Taylor bubble's lateral displacement from the tube axis were determined in single and dual bubble systems. The single bubble experiments with 7.5- and 15-cm long, bullet shaped solid bubbles with axi-symmetric and deformed nose shapes showed a significant decrease in the drag force with Taylor bubble displacement from the tube axis for all bubbles. For the deformed nose bubbles, the measured drag force was significantly smaller than for the normal nose bubbles at all lateral bubble positions. In the dual bubble system, the drag force measured on a trailing bubble at the center of the pipe increased gradually with the increasing separation distance up to about two pipe diameters, while beyond this region the drag force remained essentially constant. A one-dimensional flow model was developed and used to determine the factors responsible for drag force reduction. Based on these results, acceleration of a trailing Taylor bubble in a gas–liquid slug flow has been attributed to the reduction in drag force caused by changes in the nose shape and lateral displacement of the bubble from the vertical pipe axis.

Keywords: Slug flow; Taylor bubble; Drag; Form Drag; Friction Drag; Rise Velocity; Bubble acceleration; Bubble coalescence

1. Introduction

Slug flow is one of several two-phase flow regimes encountered in many industrial situations, for example, in the production of hydrocarbons in oil wells and their transportation in pipelines, in nuclear reactors during emergency core cooling, in boilers, condensers and chemical reactors. Sometimes, the flow is accompanied by mass and heat transfer between the gas and liquid phases.

Because of its importance in a wide variety of industries, the vertical slug flow has been studied extensively since 1940s. Dumitrescu (1943) obtained a theoretical expression for the velocity of a bullet-shaped Taylor bubble steadily rising in a stagnant liquid column assuming a potential flow field around the bubble. He also derived theoretically the Taylor bubble shape, which agrees well with the experimental data for an air–water system (e.g., Mao and Dukler, 1989) and other fluid systems such as air–kerosene (Ahmad et al., 1998). Moissis and Griffith (1962) developed an empirical correlation for the rise velocity of an accelerating Taylor bubble as an exponential function of the decreasing distance behind a leading Taylor bubble. Many other researchers have undertaken further investigations of vertical slug flow: Davies and Taylor (1950), Nicklin et al. (1962), Street and Tek (1965), Akagawa et al. (1966), Fernandes et al. (1983), Bendiksen (1984), (1985), Nickens et al. (1987), Reinelt (1987), Couet and Strumolo (1987), Mao and Dukler (1989,1990) among others.

Although extensively studied in the past several decades, certain key aspects of the vertical slug flow still remain poorly understood. For example, the mechanism is not yet clear for the acceleration of a trailing Taylor bubble and its coalescence with a preceding Taylor bubble for separation distances smaller than some critical value, which has been referred to as the minimum stable liquid slug length by Dukler et al. (1985). Dumitrescu (1943) and Davies and Taylor (1950) have shown that the radius of curvature at the stagnation point on the

* Corresponding author. Fax: 416-978-8605.
E-mail address: kawaji@ecf.toronto.edu (M. Kawaji)

0009-2509/99/$ - see front matter
PII: S0009-2509(99)00149-9

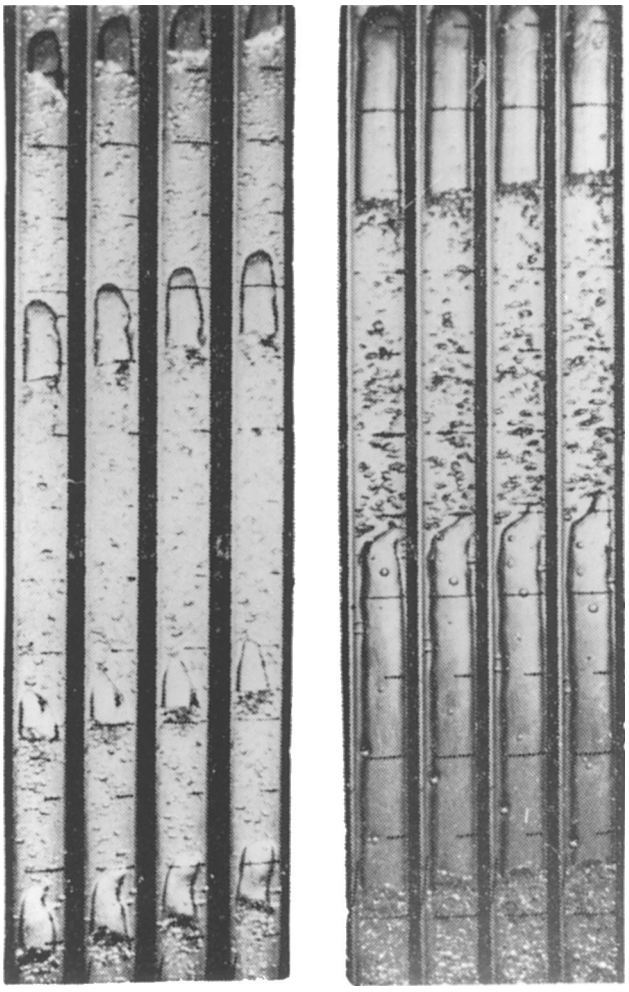

Fig. 1. Shape of Taylor bubbles in upward slug flow (from Kagawa and Kariyasaki, 1982).

nose is important in determining the Taylor bubble rise velocity in a vertical tube. Zukoski (1966) reported significant increases in the Taylor bubble rise velocity due to the inclination of a pipe and the changes in the lateral position of the bubble and the curvature of the bubble nose. Zukoski also reported that when two Taylor bubbles rise with a short separation, the flow disturbances in the wake of the leading bubble can cause large-scale distortions of the trailing bubble which leads to an increase in the rise velocity of the trailing bubble and coalescence of the two bubbles.

The deformation of the bubble nose in a developing slug flow in a vertical tube was photographed by Kagawa and Kariyasaki (1982). Their photographs (Fig. 1) clearly indicate the deformation and lateral displacement of the bubble nose from the vertical tube axis, along which the bubble nose usually lies in well-developed slug flows.

Previously, Collins et al. (1978) related the rise velocity of a Taylor bubble in a developed slug flow to the maximum liquid velocity at the tube axis. Bendiksen (1984) measured the rise velocity of Taylor bubbles in inclined tubes, and found that the rise velocity is greater in inclined tubes than in a vertical tube, as previously reported by Zukoski (1966). Shemer and Barnea (1987) observed random and alternate movements of the bubble nose from one side of the pipe to the other, in accordance with the velocity profiles at the corresponding distances ahead of the nose. Consequently they correlated the rise velocity of a Taylor bubble with the maximum instantaneous liquid velocity upstream.

The wake behind gas slugs rising through a quiescent liquid in a 19-mm ID vertical tube was studied visually by Campos and Guedes de Carvalho (1988). They observed that the wake volume became independent of the gas slug length up to 88 mm for a given tube diameter and liquid viscosity. The wake structure reported was significantly different from that of wakes behind circularly capped bubbles in an unconfined liquid reported by Bessler and Littman (1987), among others, which suggests that the presence of a tube has a strong influence on the liquid hydrodynamics and bubble rise velocity.

Recently, using the photochromic dye activation technique, Ahmad et al. (1998) and DeJesus et al. (1995) measured instantaneous velocity profiles in the liquid surrounding the leading and trailing Taylor bubbles rising in a vertical 25.6-mm ID tube. From the velocity

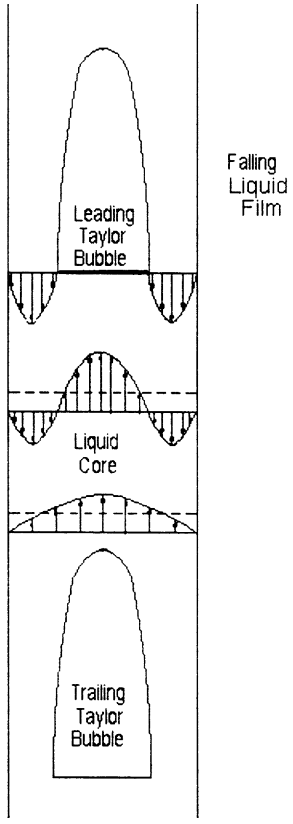

Fig. 2. Velocity profiles in the wake and acceleration of a trailing Taylor bubble.

profile measurements in the wake of a leading Taylor bubble, the wake size and the penetration distance of a liquid film falling past a Taylor bubble into its wake could be directly determined. They observed that the liquid film penetrates only less than about 2 tube diameters ($2D$), and certainly not all the way down to the trailing Taylor bubble which could, however, begin accelerating far below at separation distances greater than 6 tube diameters.

Because the downward falling film would cause an increase in the upward velocity of the liquid core, the trailing Taylor bubble can increase its rise velocity if the downward liquid flow exists near the tube wall, as illustrated in Fig. 2. However, if the liquid stops flowing downward near the tube wall at about $2D$ below the tail of the leading Taylor bubble, another mechanism must be responsible for the acceleration of the trailing Taylor bubble in the region $2D$–$6D$ below the leading Taylor bubble.

Dukler et al. (1985) previously hypothesized that there is a minimum stable slug length (or the minimum separation distance between two successive Taylor bubbles) beyond which the Taylor bubbles will rise at the same velocity and would not coalesce. They proposed a model to calculate the minimum stable slug length based on the development of a new boundary layer in the liquid slug, behind the wake of a preceding Taylor bubble. However, their hypothesis has not been experimentally verified.

DeJesus et al. (1995) and Ahmad et al. (1998) have recently suggested another mechanism for the Taylor bubble acceleration. Their as well as previous experimental observations indicated a significant deformation of the nose shape and lateral motion from one side of the tube to the other for a trailing Taylor bubble accelerating behind another Taylor bubble. Since one of the important factors controlling the rise velocity of a Taylor bubble under steady flow conditions is the drag force, the Taylor bubble would rise faster if the drag force experienced is reduced as it moves off the tube axis or the shape of the nose becomes asymmetric. Zukoski's (1966) and Bendiksen's (1984) measurements of greater rise velocities for Taylor bubbles rising in inclined tubes than in a vertical tube are consistent with the proposed mechanism since the Taylor bubbles move upward in eccentric positions in inclined tubes and the nose shape is not axially symmetric. Thus, the main objective of this work was to experimentally verify the above hypothesis for a mechanism of Taylor bubble acceleration in vertical slug flow based on the drag force reduction due to the bubble's lateral displacement and distortion of the nose shape. Considering the difficulties encountered in studying the motion of gaseous Taylor bubbles under controlled flow conditions, solid models of Taylor bubbles were used in the present work and the differences between the solid and gaseous Taylor bubbles examined in detail.

2. Experimental apparatus and procedure

The experiments have been conducted with solid models of Taylor bubbles made of acrylic resin placed in a vertical glass tube, in which a liquid was forced to flow downward. Hereafter, the "bubble" or "Taylor bubble" refers to such a solid plastic model.

As shown in Fig. 3, the solid Taylor bubble was suspended from a tension-compression load cell and placed in a downward flowing liquid stream in a vertical tube of 25.6 mm inner diameter. The analog output of the load cell (Entran ELJ-0.5N, sensitivity 115.8mV/FS, 10V excitation) was converted to a digital signal through a data acquisition board DAS-8 and an EXP16 multiplexer board with a gain of 50. LABTECH NOTEBOOK was the software utilized to collect data with a sampling frequency of 300 Hz in a personal computer with a 80486-66 MHz CPU. The time averaged value for the drag force was obtained from the data collected for a period of 30 s. The lateral position of the bubble could be adjusted using a traversing mechanism, including two micrometer heads, installed diametrically opposite to each other as shown in Fig. 4. The diameter of the Taylor bubble at the tail was 2.2 mm less than the tube inner diameter, such that when the bubble is located at the tube axis, the liquid film would be 1.1 mm thick on all sides. The bubble was traversed from the tube center towards the left and the right walls to measure any changes in the drag force. Although this system is not hydrodynamically equivalent to a cocurrent upward slug flow because the velocity profiles ahead of the Taylor bubble are different, the effect of Taylor bubble displacement from the tube axis on drag force was expected to be quite similar as the liquid film starts to fall down at the bubble nose even in cocurrent slug flow.

Two types of drag force measurements have been conducted in the present work.

(1) With a single bubble, for different lateral bubble displacement or eccentricity values. The same test procedure was followed to obtain data at six different flow rates, for two different bubble lengths, 7.5 and 15 cm, and for two different bubble nose shapes, normal and deformed, as shown in Fig. 5. The deformed bubble had a smaller radius of curvature at the stagnation point.

(2) With a two-bubble system consisting of leading and trailing plastic Taylor bubbles. The leading solid Taylor bubble was suspended along the tube axis using thin nylon wires passed through four equally distributed holes (0.1 mm ID) in the bubble's nose region, such that the bubble would not be tilted inside the tube. The trailing bubble was suspended from the load cell in the wake of the leading bubble using another nylon wire. This wire was passed through a centrally positioned hole in the leading Taylor bubble, so that the two bubbles are aligned along the tube axis. Two sets of runs have been performed: the first consisted of drag force measurements

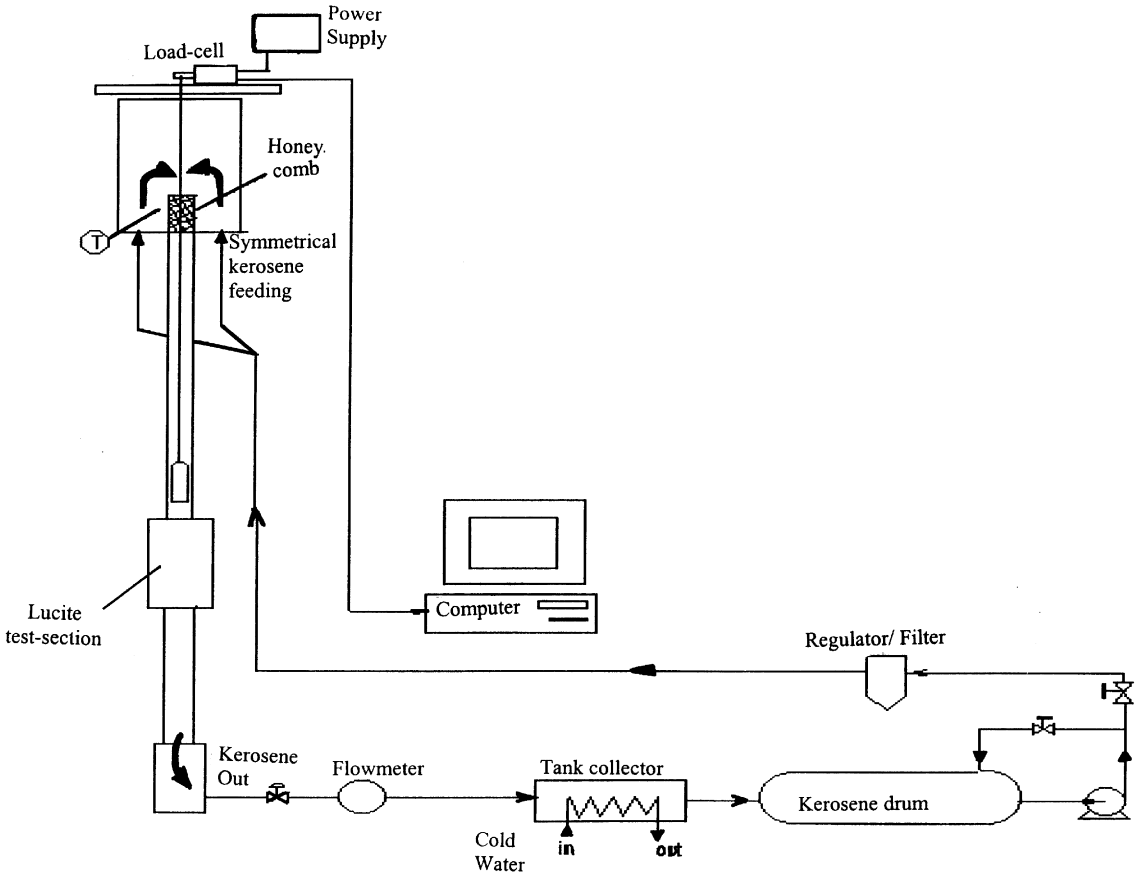

Fig. 3. Test loop for drag force measurements.

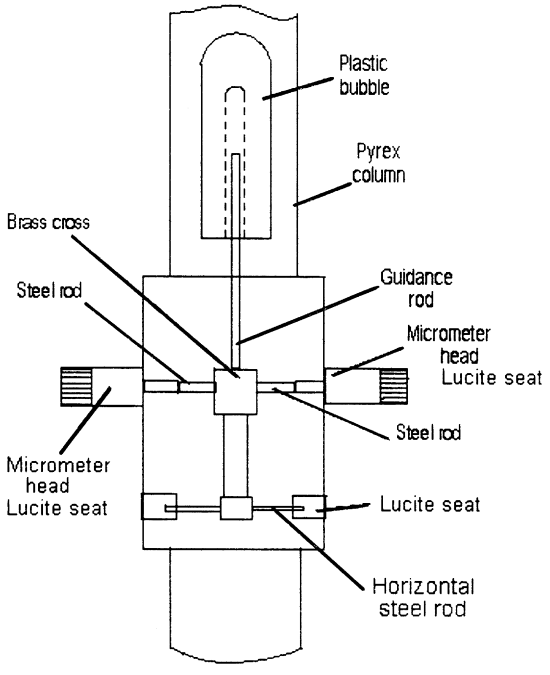

Fig. 4. Solid bubble traversing mechanism.

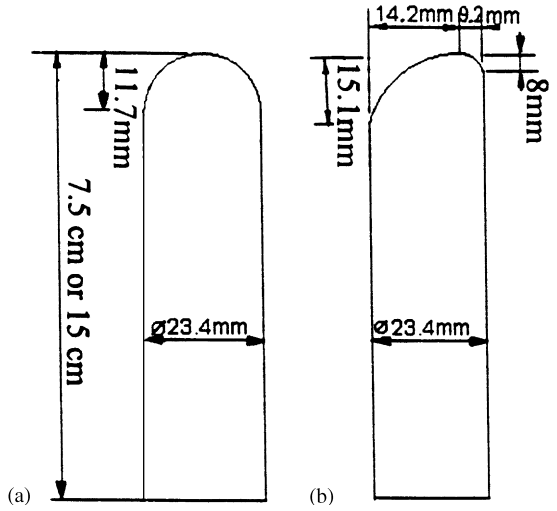

Fig. 5. Plastic Taylor bubbles: (a) normal, (b) deformed.

on the trailing bubble for different separation distances from $z = 0$ to $9D$ with both bubbles located at the tube axis, and the second was the drag force measurement on the trailing bubble at different lateral positions for three different bubble separation distances, $z = 3D$, $5D$ and $7D$.

It is important to mention that the force measured by the load-cell was actually the resultant force of buoyancy and total drag. For each bubble, the buoyancy force was determined from the load-cell measurement of the solid Taylor bubble being suspended in a stagnant column of kerosene. This force was then subtracted from the actual load-cell readings for the dynamic system to obtain only the total drag force on the bubble.

The range of the liquid flow rates was selected to cover the experimental rise velocities obtained for an air–kerosene system, for both single and trailing bubble configurations, i.e. liquid Reynolds numbers (based on mean liquid velocity and tube diameter) between 2200 and 4349, corresponding to rise velocities of about 14.9–29.4 cm/s. The details of the experimental procedure and measurement technique can be found in Tudose (1997).

3. One-dimensional flow model

The variation of the drag force with the lateral displacement of the Taylor bubble was evaluated using a one-dimensional model based on continuity, momentum and mechanical energy equations, with appropriate head losses taken into account. A model of Liu and Richards (1994) developed for capsule transport in a pipeline was followed with some modifications for the present problem.

The geometry of flow past a solid bubble modeled is shown in Fig. 6. The solid Taylor bubble of diameter, D_{TB}, is positioned as shown inside a pipe of inner diameter, D. The bubble eccentricity, e, is defined as the ratio of the displacement of the bubble axis from the pipe axis to the difference between the bubble and pipe radii, and varies from 0 (concentric bubble) to ± 1 (fully eccentric bubble). The bubble nose is semispherical and forms a converging channel (Sections 1 and 2 in Fig. 6) with the pipe wall. The liquid flows downward from above the nose (Section 1) with a fully developed turbulent velocity profile, past the nose region (Sections 1 and 2) and through a concentric or eccentric annulus (Sections 2 and 3).

The pressure difference between the nose and tail of the solid Taylor bubble is given by the hydrostatic head and various head-losses:

$$\frac{p_1 - p_3}{\rho_L} + g(z_1 - z_3) = K\frac{u_1^2}{2} \tag{1}$$

where p_1 and p_3 are the static pressures at the nose and tail of the solid Taylor bubble, respectively, ρ_L is the liquid density, g is the gravitational acceleration, z is the elevation, K is the total head-loss coefficient, and u_1 is the mean liquid velocity in the pipe. The value of K can be estimated from the entrance head-loss coefficient, K_{en},

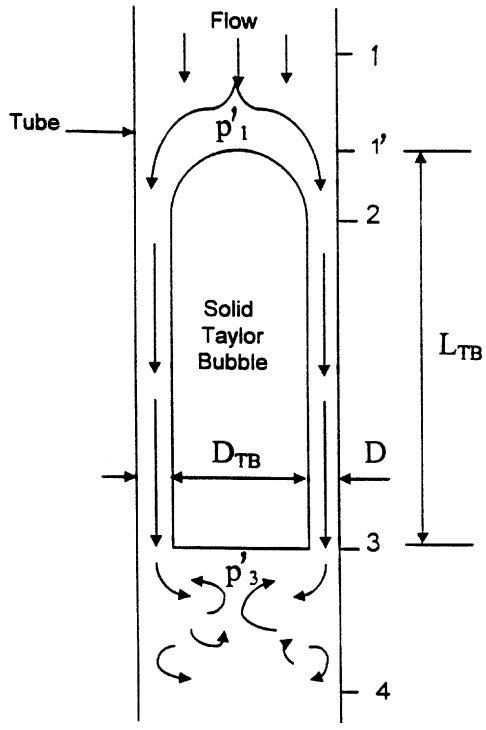

Fig. 6. Geometry used in the one-dimensional model.

in the nose region, skin friction in the annulus along the side of the Taylor bubble, and changes in the flow channel geometry and velocity profiles.

The head-loss in the nose region was modeled by a loss coefficient, K_{en}, for a reducer with gradual contraction in the cross-sectional area from a circular pipe to that of an annulus formed by the pipe inner wall and the solid Taylor bubble:

$$\frac{p_1 - p_2}{\rho_L} + g(z_1 - z_2) = \frac{1}{2}(\alpha_2 u_2^2 - \alpha_1 u_1^2) + K_{en}\frac{u_2^2}{2} \tag{2}$$

Here, α_1 and α_2 are the kinetic energy correction factors for turbulent flow in a circular pipe and laminar flow in an annulus, respectively. For the present cross-sectional area ratio, the entrance head-loss coefficient, $K_{en} = 0.18$, for a reducer with an included angle of about 90° was used (Fox and McDonald, 1992). Although lateral displacement of the bubble nose is expected to have some effect on the entrance head-loss coefficient due to the changes induced in the liquid streamlines, no useful data could be found in the literature to represent this effect. Thus, in the present model, K_{en} was assumed to remain constant for all bubble displacements.

The kinetic energy correction factor, α_1, for turbulent flow in the circular pipe upstream of the bubble nose can be taken as 1.0. On the other hand, the value of α_2 for flow at the entrance of an annular region (Section 2 in Fig. 6) cannot be accurately estimated since the velocity

profile is changing from a fully developed turbulent profile above the nose to a developing laminar velocity profile in an annulus at the end of the converging section. For a fully developed laminar flow in a concentric annulus with a diameter ratio close to 1, the value of α_2 would be equal to 1.54, which is taken to be the same as for flow between parallel plates (Streeter, 1961). If the velocity profile were, however, still developing, then the value of α_2 should be less than 1.54. The value of α_2 would also vary with the lateral displacement of the bubble. Liu and Richards (1994) developed a correlation for fully developed flow in a fully eccentric annulus, $e = 1$, from Jonsson and Sparrow's (1966) work on flows in eccentric annuli,

$$\alpha = 1 + 0.193k + 0.0763k^2 \tag{3}$$

where k is the ratio of the Taylor bubble diameter, D_{TB}, to the pipe diameter, D. For the present experiment, the value of k is 0.91 and Eq. (3) gives $\alpha_2 = 1.24$. The actual value would again be smaller for a developing flow, thus the value of α_2 was assumed to be equal to 1.24 for all lateral positions of the bubble in the present model. This could lead to slight underestimation of α_2 at $e = 0$ and overestimation at $e = \pm 1$.

The friction pressure drop between the entrance and exit of the annulus (Sections 2 and 3) was estimated using a friction factor, f_{sk}, for laminar flow in a concentric or eccentric annulus,

$$\frac{P_2 - P_3}{\rho_L} + g(z_2 - z_3) = f_{sk}\left[\frac{L_{TB} - D_{TB}/2}{D - D_{TB}}\right]\frac{u_2^2}{2} \tag{4}$$

where L_{TB} is the Taylor bubble length. A blockage ratio is defined using the diameter ratio, k, as follows.

$$b = 1/(1 - k^2). \tag{5}$$

From the continuity equation, the mean velocities in the pipe and annulus can be related by this blockage ratio, as follows:

$$u_2 = bu_1. \tag{6}$$

By using Eq. (6) and comparing Eqs. (1), (2) and (4), the overall head-loss coefficient can be written as

$$K = b^2\left[(\alpha_2 + K_{\text{en}}) + f_{sk}\frac{L_{TB}}{D - D_{TB}}\right] - 1. \tag{7}$$

The friction factor, f_{sk}, for laminar flow in an eccentric annulus was also calculated using Liu and Richards' (1994) correlation with a modification made to take into account the effect of bubble eccentricity, e, derived theoretically by Tiedt (1967).

$$f_{sk} = \frac{C_1}{Re_f(1 + 1.5e^2)}. \tag{8}$$

The coefficient, C_1, is given by

$$C_1 = 48 + 3348(k - 0.75)^{3.07}. \tag{9}$$

The Reynolds number for flow in the annulus, Re_f, is defined using the mean velocity in the annulus and the hydraulic diameter, which is equal to $(D - D_{TB})$. For the range of liquid flow rates tested, the values of Re_f remained below 2300 which can be regarded as the critical Reynolds number for laminar to turbulent flow transition in both the concentric and eccentric annuli (Hanks, 1963).

The total drag force acting on the solid Taylor bubble, f_D, consists of form drag, $(f_D)_{\text{form}}$, caused by the pressure difference and friction drag, $(f_D)_{\text{skin}}$, due to the shear stress. For the form drag calculation, the effect of pressure increase due to flow stagnation at the nose, $p_1' - p_1$, can be estimated using a pressure coefficient, C_p, which decreases from 1.0 to less than -1.0 around the nose at Section 2. Since the average value of C_p would be close to 0 and relatively small compared to other head-loss terms, the form drag was calculated without C_p using,

$$\begin{aligned}(f_D)_{\text{form}} &= (p_1' - p_3)A_{TB} - \rho g A_{TB}L_{TB} \\ &= \left\{b^2\left[(\alpha_2 + K_{\text{en}}) + f_{sk}\left(\frac{L_{TB} - \frac{D_{TB}}{2}}{D - D_{TB}}\right)\right] - 1\right\}A_{TB}\frac{\rho u_1^2}{2}.\end{aligned} \tag{10}$$

The friction drag was calculated from,

$$\begin{aligned}(f_D)_{\text{skin}} &= \tau_{TB}L_{TB}\pi D_{TB} = \frac{b^2(1 - k^2)}{k(k + \phi_1)} \\ &\quad\left[(\alpha_2 + K_{\text{en}}) + f_{sk}\left(\frac{L_{TB} - \frac{D_{TB}}{2}}{D - D_{TB}}\right) - 1\right]A_{TB}\frac{\rho u_1^2}{2}\end{aligned} \tag{11}$$

where A_{TB} is the cross-sectional area of the Taylor bubble at the tail, and ϕ_1 is the ratio of the shear stresses at the pipe wall and the solid bubble surface, $\phi_1 = \tau_w/\tau_{TB}$. This shear stress ratio is given by the following equations for a fully eccentric annulus, $e = 1$:

$$\phi_1 = \sqrt{1 - (1 - k)^2} \tag{12}$$

and for a concentric annulus, $e = 0$ (Liu and Richards, 1994),

$$\phi_1 = \frac{k(2\ln k - k^2 + 1)}{k^2 - 1 - 2k^2\ln k}. \tag{13}$$

For the present bubble to tube diameter ratio, $k = 0.91$, the values of ϕ_1 given by Eqs. (12) and (13) differed by less than 3%, which would cause at most a 1% difference in the friction drag force calculated from Eq. (11). Thus, Eq. (12) was used for all the eccentricity values in the present calculations.

Although not considered in the present drag force calculation, the pressure recovery in the wake behind the solid Taylor bubble can be estimated using an exit head-loss coefficient, K_{ex}, as follows:

$$\frac{p_3 - p_4}{\rho_L} + g(z_3 - z_4) = \frac{1}{2}(u_4^2 - \alpha_3 u_3^2) + K_{\text{ex}}\frac{u_2^2}{2}. \tag{14}$$

Liu and Richards (1994) developed a correlation for the exit head-loss from an analysis of flow expansion from a fully eccentric annulus to a circular pipe using continuity, momentum and energy equations,

$$K_{ex} = \alpha - (2b\beta - 1)/b^2. \quad (15)$$

Here, β is the momentum correction factor for laminar flow through an annulus. For a concentric annulus, $\beta = 1.20$ (Streeter, 1961). For a fully eccentric annulus, Liu and Richards (1994) developed the following correlation from Jonsson and Sparrow's (1966) work:

$$\beta = 1 + 0.061k + 0.044k^2. \quad (16)$$

For the present value of $k = 0.91$, the value of β is 1.09. If an average β value of 1.15 is used along with the kinetic energy correction factor, α_3, which is assumed to have the same value as α_2(= 1.24), Eq. (15) gives $K_{ex} = 0.89$. This value was used in the estimation of the pressure recovery in the wake for all values of bubble eccentricity.

In the present drag force calculation, the exit head-loss and pressure recovery were not included, because the pressure recovery takes place over a certain distance behind the Taylor bubble tail, and the pressures acting on the bubble tail (p'_3) and at the exit of the annulus, p_3, can be assumed to be equal (Liu and Richards, 1994). A possible effect of the exit head-loss and pressure recovery in the wake on the drag force calculation was nevertheless evaluated by comparing the magnitudes of total drag forces calculated with and without the pressure difference, $p_3 - p_4$, included in the overall pressure difference between the nose and tail of the solid Taylor bubble.

4. Results and discussion

4.1. Effect of lateral displacement of a single Taylor bubble

For six different liquid flow rates between $Re = 2200$ and 4349, the drag force on a 15-cm long solid Taylor bubble was measured for incremental displacement of the bubble from the tube axis. The data for $Re = 2428$ and 4349 are shown in Fig. 7a and Fig. 7b, respectively. In these and other four cases, there was a gradual but significant decrease in the drag force with bubble eccentricity. The drag force profiles were characterized by reasonably good symmetry with a peak located at the center of the tube (zero eccentricity) and minimum values when the bubble is touching the tube wall (eccentricity = ± 1).

Fig. 7a and Fig. 7b, as well as other figures in this paper also contain drag coefficient values calculated from the measured drag force, f_D,

$$C_D = 2\frac{f_D}{\rho u^2 A_{TB}}. \quad (17)$$

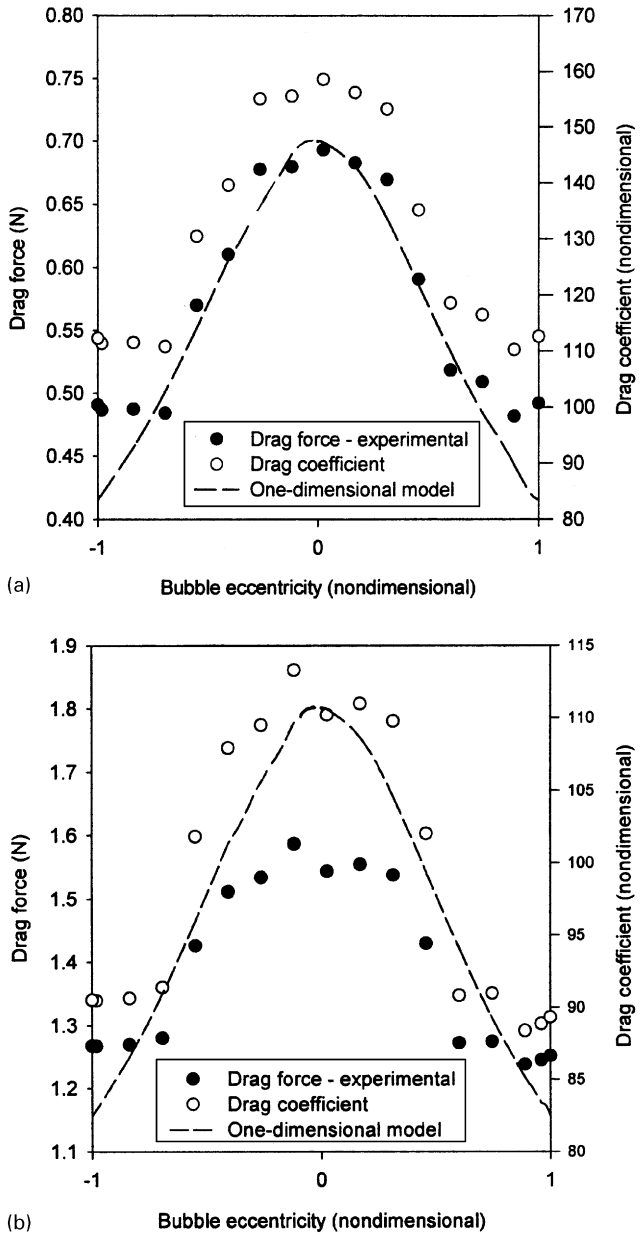

Fig. 7. Drag force and drag coefficient variations with lateral displacement for a 15-cm Taylor bubble with a normal nose (a) $Re = 2428$, (b) $Re = 4349$.

The drag coefficient for a gaseous Taylor bubble cannot be easily estimated and compared with the present data, since the pressure is nearly constant inside the gas bubble and along the liquid film, and thus the drag and buoyancy forces are not readily separable as will be discussed in a later section.

A physical explanation for significant reductions in the drag force with lateral bubble displacement is provided by the predictions of the one-dimensional model, which are shown by a dashed curve in Fig. 7a and Fig. 7b. The model is seen to predict the drag reduction with lateral bubble displacement quite well for these liquid flow rates

($Re = 2428$, $Re_f = 1272$; $Re = 4349$, $Re_f = 2278$), although the drag forces for $Re = 4349$ are overestimated at small eccentricity values.

The model predictions for $Re = 2428$ show that for a concentric bubble, the head-loss due to a converging flow in the nose region is about a half of the loss due to friction in the annulus (33% vs. 68%). These entrance and friction losses result in the form and friction drag forces of 0.64 N and 0.064 N, respectively, at the concentric position. As the bubble is displaced laterally to fully eccentric positions, $e = \pm 1$, the friction pressure drop in the annulus decreases significantly, down to approximately 45% of the total head-loss. This reduction in skin friction is calculated to cause 40% reductions in the form drag from 0.64 N to 0.38 N, friction drag from 0.064 N to 0.038 N and the total drag force, from 0.70 N to 0.42 N. Thus, the reduction in the total drag force with the lateral displacement of the solid Taylor bubble is believed to occur primarily due to the reduction in the friction pressure drop in the annulus between the solid Taylor bubble and the pipe wall.

The bubble nose eccentricity is expected to also affect the entrance head-loss coefficient, K_{en}, and the kinetic energy correction factor, α_2, which were assumed to be constant in the present model, however, the reduction in the friction pressure drop in the annulus appears to be sufficient to explain the total drag force reductions observed with the lateral displacement of the solid Taylor bubble for the runs examined.

4.2. Influence of Taylor bubble length

The drag force measurements have been performed for the 7.5-cm long bubble, as indicated in Fig. 8 over the same range of flow rates as for the 15-cm long bubble. Similar drag force variations were obtained for the two bubbles of different lengths. However, a comparison of the drag force data for the two bubble lengths indicates smaller values for the shorter bubble, as shown in Fig. 9. The smaller total and form drag for the shorter bubble can be attributed to a smaller friction pressure drop in the shorter annulus. The flow in the annulus was laminar at all liquid flow rates tested for both bubble lengths and nearly fully developed at the bubble tail even for the 7.5-cm long bubble. Thus, a lower pressure at the tail of the longer bubble due to a greater friction pressure drop in the annulus resulted in greater form and total drag forces for the longer bubble.

4.3. Influence of bubble nose shape

When the nose of gaseous Taylor bubbles becomes distorted, the bubbles have been observed to accelerate (Zukoski, 1966). Thus, experiments identical to those described in the previous sections have been performed with 7.5 and 15-cm long solid Taylor bubbles with a deformed nose shape. For both the 7.5-cm and 15-cm long bubbles with a deformed nose, smaller drag forces were obtained in comparison with the normal nose bubbles. For the 7.5 cm bubble, the reduction in the drag force due to nose deformation was approximately 30% for all values of bubble eccentricity, as shown in Fig. 10. It is clear that the total drag force is reduced by deformation

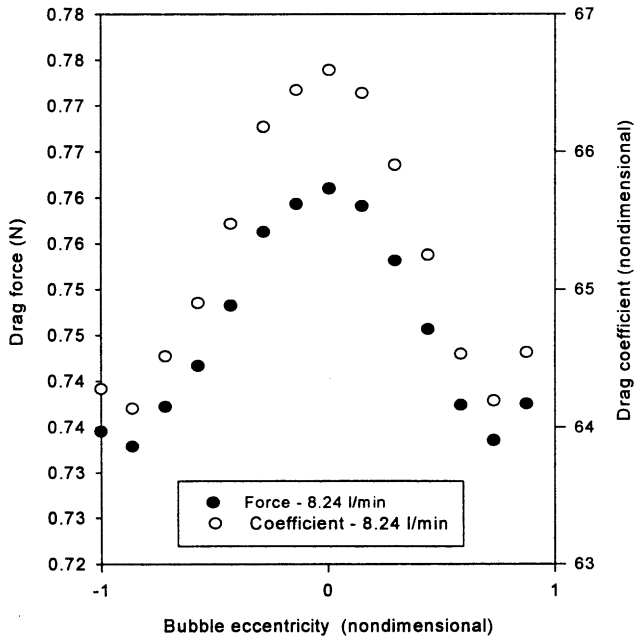

Fig. 8. Drag force and drag coefficient variations with lateral displacement for a 7.5-cm Taylor bubble with a normal nose ($Re = 3954$).

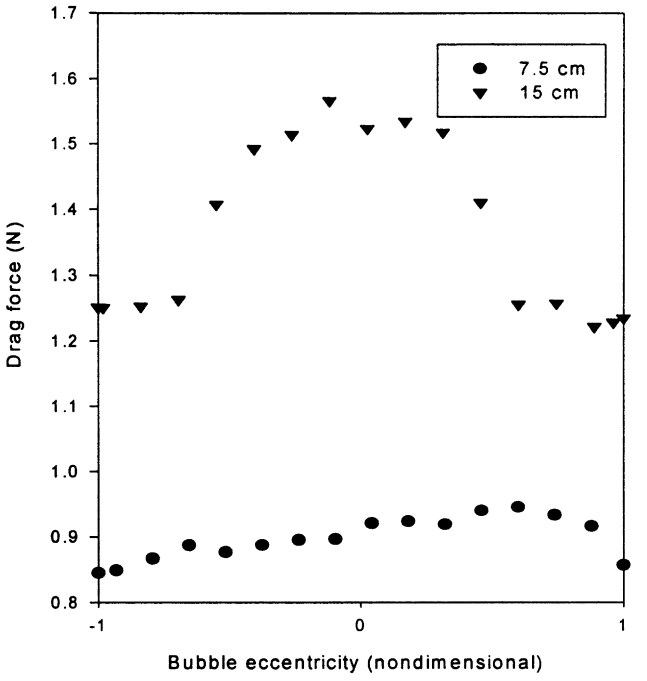

Fig. 9. Drag force comparison between 7.5-cm and 15-cm Taylor bubbles at $Re = 4349$.

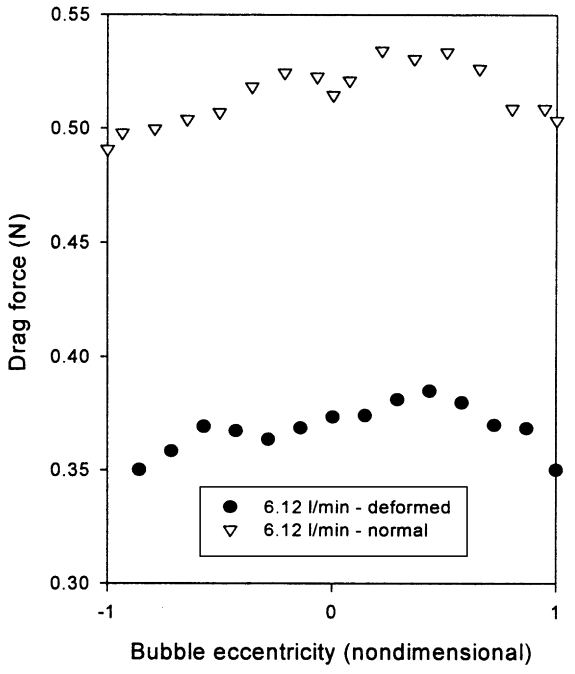

Fig. 10. Drag force variations with lateral displacement for 7.5-cm long Taylor bubbles with normal and deformed nose.

of the bubble nose as the asymmetric nose diverts more liquid to one side of the bubble and alters the streamlines in the nose region as well as the circumferential liquid flow rate distribution in the annulus.

Further reduction in the drag force due to the lateral displacement of the deformed bubble is attributed to the reduction in friction pressure drop in the eccentric annulus as discussed earlier. The constant difference between the measured drag forces for the normal and deformed bubbles at all values of eccentricity suggests that the effect of the altered liquid streamlines in the nose region remains relatively unchanged at all lateral positions of the bubble.

From the modeling point of view, the form drag reduction due to the changes in the liquid streamlines in the deformed nose region can be accounted for by a reduction in the entrance head-loss term involving K_{en} and α_2, or the friction pressure drop term in Eq. (11). The friction pressure drop in the annulus, however, should not be significantly different between the deformed and normal nose bubbles, since the friction factor remains unchanged for the same annulus geometry. Although there may be a small effect of non-uniform liquid flow distribution in the annulus on the friction pressure drop, it is unlikely the cause of the 30% reduction in the measured drag force. Thus, it is more reasonable to think that the entrance loss term decreases in value for the deformed nose bubble, which led to the 30% reduction in the total drag force. Introduction of eccentricity-dependent entrance head-loss and kinetic energy correction factors would be necessary to predict the deformed bubble results.

The deformed bubble results have a significant implication for application of the present work to the gaseous Taylor bubbles. The free surface of gaseous Taylor bubbles would respond to any pressure fluctuations. The nose shape can continuously change if the pressure field in the vicinity of the bubble nose is non-uniform and unsteady, due to the small-scale eddies remaining well below the immediate wake of the preceding Taylor bubble. Nose deformation will then alter the liquid streamlines in the nose region and should reduce the entrance head-loss as observed in the deformed solid Taylor bubble results. As will be discussed in a later section, the friction pressure drop in the annulus region will be negligibly small in the case of gaseous Taylor bubbles, and the entrance head-loss in the nose region determines the overall drag force. Since the liquid streamlines are expected to be similar in the deformed nose regions of solid and gaseous Taylor bubbles, the reduction in the entrance head-loss observed for the solid Taylor bubbles is also expected for the gaseous Taylor bubbles. Thus, acceleration of gaseous Taylor bubbles due to the deformation of the nose shape reported in the past literature can be attributed to a change in the liquid streamlines in the nose region that reduces the drag force as observed in the present experiments with deformed solid Taylor bubbles.

4.4. Influence of leading bubble on trailing bubble

With two solid Taylor bubbles aligned along the vertical tube axis, measurements of the drag force on the trailing bubble were made at different separation distances. As shown in Fig. 11, there were two regions in which the drag force varied in a different manner. In the wake region just below the leading Taylor bubble ($z < 2D$, where z is the downward distance measured from the tail of the leading Taylor bubble), the drag force on the trailing bubble increased rapidly with the separation distance. In the second region further behind the leading Taylor bubble ($z > 2D$), the drag force gradually decreased slightly or remained almost constant regardless of the separation distance.

The variation of the drag force on the trailing bubble as a function of the distance from the leading Taylor bubble obtained in the present work is consistent with the rise velocity data obtained and correlated by Moissis and Griffith (1962). In their correlation, the rise velocity remained constant until the trailing Taylor bubble's nose came within about 6 tube diameters of the leading Taylor bubble's tail. The rise velocity then increased gradually at first and then rapidly as the separation distance decreased to less than $2D$ due most likely to a significant reduction in the drag force.

To show that the direct effect of the leading Taylor bubble's wake is limited to the near tail region ($z < 2D$) only, further drag force measurements were performed

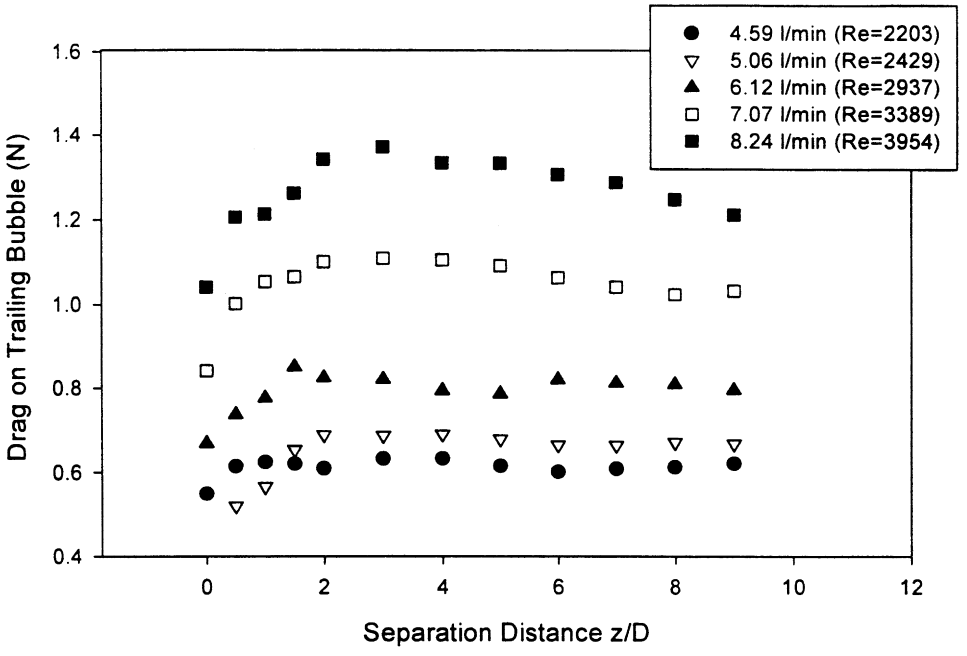

Fig. 11. Variation of the drag force with the separation distance for a 15-cm long trailing Taylor bubble behind a 15-cm leading Taylor bubble.

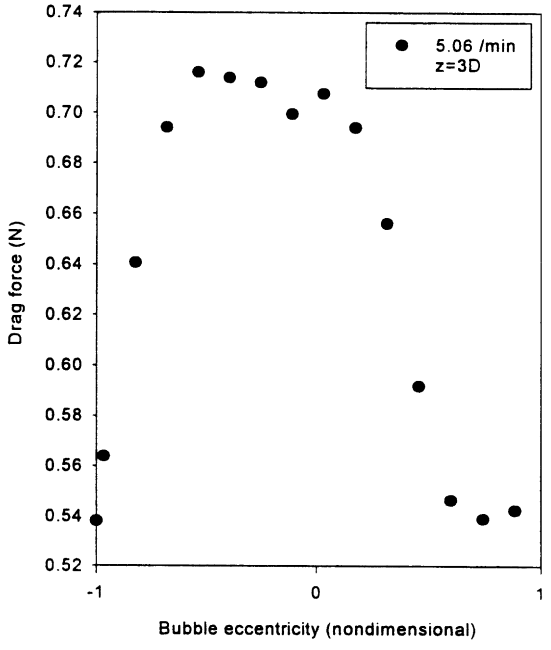

Fig. 12. Drag force variation with lateral displacement for a 15-cm long trailing bubble with a normal nose at $z = 3D$ from the 15-cm leading bubble.

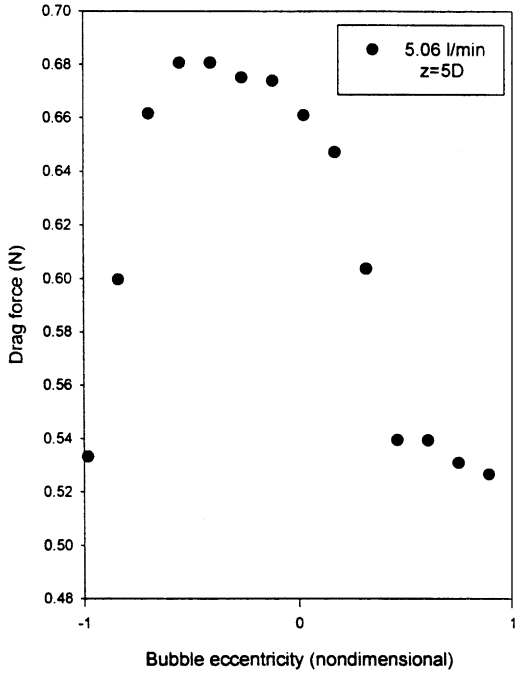

Fig. 13. Drag force variation with lateral displacement for a 15-cm long trailing bubble with a normal nose at $z = 5D$ from the 15-cm leading bubble.

for the trailing Taylor bubble laterally displaced from the tube axis, as shown in Figs. 12–14. The drag force profiles obtained at $z = 3D$, $5D$ and $7D$ were similar to those for a single bubble, showing a peak at the tube center and a significant decrease as the bubble is laterally displaced. Also, a comparison of the maximum drag force recorded for single and trailing bubble configurations, at different separation distances and flow rates, revealed similar values, as shown in Fig. 15.

In view of the constant drag force observed outside the immediate wake region ($z > 2D$) for the axially centered trailing bubble in the present work, it is reasonable to think that for gaseous Taylor bubbles, the acceleration of

the trailing bubble starting from far below the leading Taylor bubble is not due to the significantly reduced pressure field in the immediate wake region ($z < 2D$). It is also useful to mention here, that for a system of two gaseous Taylor bubbles rising through stagnant kerosene in a 25.6 mm ID tube, visualization of the flow field behind the leading Taylor bubble by DeJesus et al. (1995) and Ahmad et al. (1998) using a photochromic dye activation technique showed a rapid decay of large vortices in only two tube diameters below the leading Taylor bubble's tail, while at four diameters below the tail, the vortex motion became totally negligible. The wake region below the leading bubble up to $z = 4D$ was characterized by the presence of large and small eddy structures (DeJesus et al., 1995).

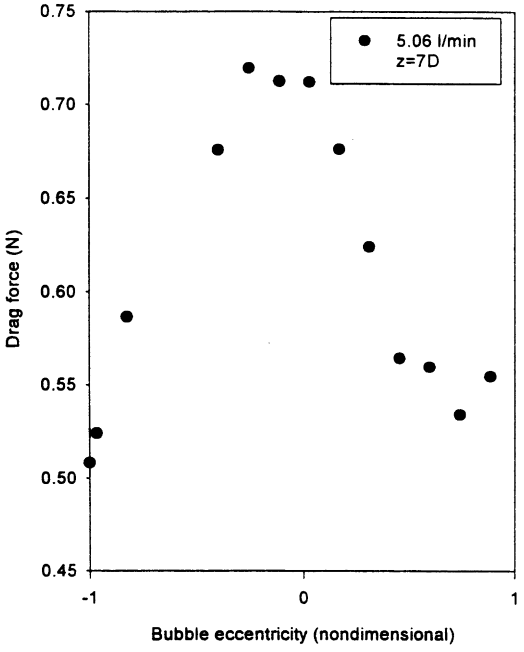

Fig. 14. Drag force variation with lateral displacement for a 15-cm long trailing bubble with a normal nose at $z = 7D$ from the 15-cm leading bubble.

A considerable degree of similarity between the gaseous and solid Taylor bubbles was not initially expected, considering that even if the geometrical similitude is satisfied and Reynolds numbers are the same for the two systems, the boundary conditions at the bubble surface are different, so the liquid film hydrodynamics should not be quite the same as will be discussed in more detail in the next section. However, the present results show that the differences between the boundary conditions at the gas–liquid interface and solid bubble surface for the liquid film entering the bubble wake do not appear to cause major modifications of the wake. Moissis and Griffith (1960) also found that the velocity profile behind an air bubble attached to the tail of a solid Taylor bubble remained identical to that obtained behind the solid tail.

4.5. Similarities and differences between gaseous and solid Taylor bubbles

To facilitate the comparison between gaseous and solid Taylor bubbles, the case of a gaseous Taylor bubble rising in a vertical tube with a downward flowing liquid will now be considered. If the volumetric flow rate of the liquid is properly adjusted, the gaseous Taylor bubble could be held stationary just as in the present experiments conducted with a solid bubble.

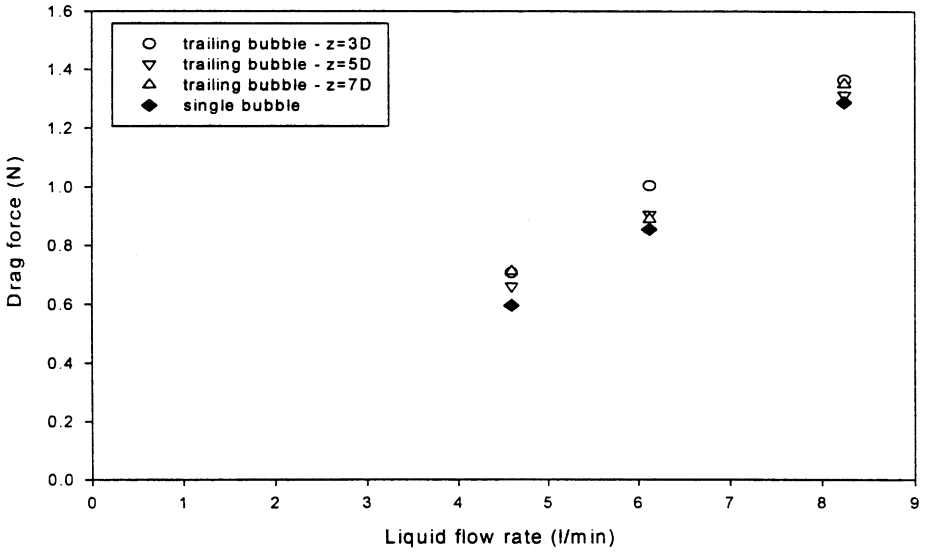

Fig. 15. Maximum drag force for single and trailing Taylor bubbles at different separation distances and liquid flow rates.

There are two major differences in the hydrodynamics between solid and gaseous Taylor bubbles, namely the absence of interfacial shear at the gas bubble surface and essentially no pressure variation in the liquid film along the gaseous Taylor bubble length. Although the friction drag estimated for the solid Taylor bubble using Eq. (11) represented only about 10% of the total drag force measured for the run shown in Fig. 7a, it is clear that the absence of interfacial shear at the gaseous Taylor bubble surface would result in a different velocity profile across the liquid film compared to that obtained in an annulus bounded by a solid Taylor bubble and a tube wall. If internal circulation is small, the pressure variation inside the gaseous Taylor bubble below the nose region would be equal to the hydrostatic head of the gas, which is small due to the small density of gas, causing little pressure variation along the falling liquid film. Then, the pressure acting on the bubble's tail would be independent of the bubble length, which results in a constant rise velocity of gaseous Taylor bubbles regardless of the bubble length (e.g. 17.5 cm/s for $D = 25.6$ mm, predicted theoretically and confirmed experimentally by Dumitrescu (1943), Mao and Dukler (1989) and DeJesus et al. (1995)). Additionally, little dependence of the wake size on the Taylor bubble length has been observed for gaseous Taylor bubbles longer than 60 mm in a 25.6 mm diameter tube (DeJesus et al., 1995), and for Taylor bubbles of length between about 30 mm up to 88 mm in a 19 mm tube by Campos and Guedes de Carvalho (1988).

If the Taylor bubble is more than several tube diameters long, the liquid film flowing downward past the side of the Taylor bubble would resemble a freely falling film in a circular tube (Ahmad et al., 1998). The film flow would be eventually governed by a balance of gravitational and viscous forces, as given by Nusselt's (1916) film theory for laminar flow (Batchelor, 1967). According to Nusselt's theory, the volumetric flow rate per unit perimeter, Γ_f, is proportional to the cubic power of the film thickness, δ:

$$\Gamma_f = g(\rho_L - \rho_G)\delta^3/3\mu_L. \tag{18}$$

On the other hand, if the Taylor bubble is long and the liquid film flow becomes turbulent, the flow rate – film thickness relationship should change. For a freely falling, turbulent liquid film in a circular tube, the flow rate – film thickness data obtained and reported by Karimi and Kawaji (1998) indicate,

$$\Gamma_f \propto \delta^{1.87}. \tag{19}$$

Thus, assuming that Eq. (18) or Eq. (19) holds locally for any film thickness, $\delta(\theta)$, the total liquid film flow rate, Q_f, for an eccentric Taylor bubble can be estimated by integrating Eq. (18) or Eq. (19) around the tube circumference for any given bubble eccentricity and liquid film thickness profile.

Since the rise velocity of a Taylor bubble, U_{TB}, can be approximately related to the total liquid film flow rate and the cross sectional area of the Taylor bubble, A_{TB}, by continuity,

$$U_{TB} = Q_f/A_{TB} \tag{20}$$

the rise velocity variation with bubble eccentricity can be readily estimated. The normalized increase in the rise velocity for a gaseous Taylor bubble with the tail diameter of 23.4 mm in a tube of 25.6 mm diameter was computed as a function of the bubble eccentricity, and is shown in Fig. 16. Predictions based on both laminar and turbulent film flow rates show significant increases in the rise velocity of a gaseous Taylor bubble as the bubble moves off the tube axis. In reality, the gaseous Taylor bubble is not expected to move laterally to fully eccentric positions ($e = \pm 1$), and the overall increase in the rise velocity would further depend on the speed and frequency of Taylor bubble's lateral motion as well.

It is worthwhile to note here for the modeling purposes that the drag and buoyancy forces cannot be separately considered for a gaseous Taylor bubble as mentioned earlier. If the buoyancy force were defined conventionally as the product of the mass of the displaced liquid and gravitational acceleration, then it would be proportional to the volume or the length of the Taylor bubble. The fact that the rise velocity of a gaseous Taylor bubble does not depend on the Taylor bubble length would then necessi-

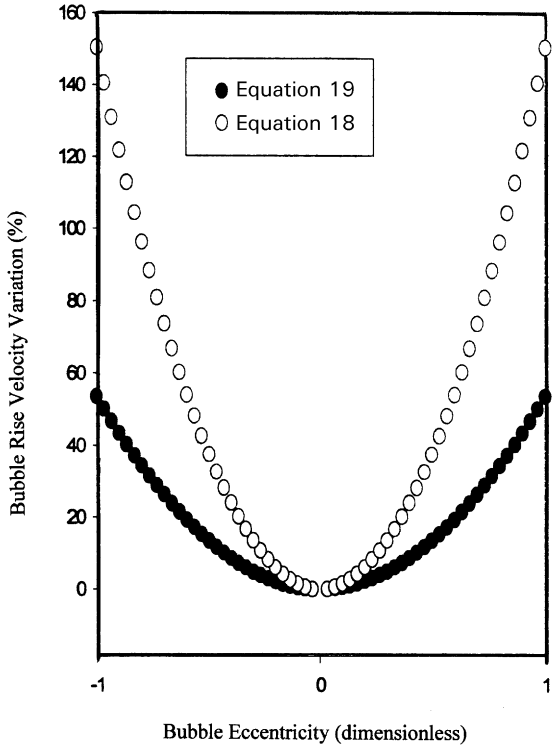

Fig. 16. Estimated variation of Taylor bubble rise velocity with lateral displacement.

tate increases in the drag force with the bubble volume or length. Furthermore, the required increase in the drag force would have to exactly match the increase in the buoyancy force, which is unlikely. Thus, we need to consider the net force due to buoyancy and drag in the case of gaseous Taylor bubbles. This net force due to buoyancy and drag for a gaseous Taylor bubble remains unchanged despite any increase in the bubble length or volume, if the Taylor bubble rises along the tube axis. It is, however, clear from the present experiments and analysis that with the lateral displacement of both solid and gaseous Taylor bubbles, the liquid encounters less hydraulic resistance and can flow downward past the Taylor bubble at a greater flow rate. This would in turn result in a greater rise velocity for the off-centered Taylor bubbles. This mechanism is consistent with the increased rise velocities of Taylor bubbles in inclined tubes as reported by Zukoski (1966) and Bendiksen (1984), since the bubbles move off-center closer to the upper tube wall and the liquid streamlines are changed in inclined tubes. Although their smallest tube inclination from the vertical was relatively large ($\sim 25^\circ$), our recent measurements of gaseous Taylor bubble's rise velocity in a 25.6 mm ID tube inclined at 5 and 15° from the vertical have also shown increases of 18 and 24%, respectively. These measurements were made with air and kerosene using a video camera and the same test section as described in Ahmad et al. (1998).

From the modeling point of view, the drag force on a gaseous Taylor bubble would arise only from a pressure difference in the nose region as the friction pressure drop term in the form drag equation will be negligibly small. Thus, the dependence on the bubble eccentricity must be clearly established for the pressure coefficient, C_p, the entrance head-loss coefficient, K_{en}, and the kinetic energy correction factor, α_2, at the end of the nose region. Accurate estimation of such dependence would require an analytical or numerical solution of three-dimensional flow field around an off-centered bubble nose, given the flow conditions above the nose.

The effect of pressure recovery in the wake was not considered in the drag force model developed for the present experiments. The pressure recovery in the wake tends to reduce the form drag estimation and although not shown, the present model of the exit head-loss given by Eqs. (14)–(16) yielded 6–10% reduction in the form and total drag forces for the run shown in Fig. 7a, as the bubble eccentricity was changed from 0 to ± 1. This resulted in an under-prediction of the measured total drag force, although the lateral variation was again well predicted. The contribution of the pressure recovery in the wake to the total drag force is thus believed to be quite small and the changes in the wake structure below its own tail are expected to have minor effects on the drag force and rise velocity of the Taylor bubble.

4.6. Why do the Taylor bubbles accelerate and coalesce?

The present results suggest that there are two effects that the wake below the tail of a leading Taylor bubble could have on the motion of a trailing Taylor bubble; (a) a direct effect, manifesting in the immediate wake of the bubble tail ($0 < z < 2D$), due to a low pressure field because of large vortices and intense mixing, and (b) an indirect effect caused by the presence of small scale, residual eddies remaining far below the tail of the leading Taylor bubble ($2D < z < 6D$). For the latter region, as long as the trailing Taylor bubble remains positioned at the center of the tube, it will experience the same drag force as the single, isolated Taylor bubble. Only when this trailing bubble is laterally displaced, there would be a significant change in the net buoyancy/drag force and an increase in the rise velocity.

The small eddies are also responsible for local variations in pressure which would influence the shape of the Taylor bubble nose. When the nose deforms in shape, the liquid streamlines in the nose region will change, affecting the pressure variation in the liquid and possibly causing a lateral motion of the trailing Taylor bubble as well. Although further studies are needed to confirm the mechanism of Taylor bubble acceleration in vertical slug flow with cocurrent liquid flow, the physics involved may be still simple and essentially the same as discussed in this paper.

Finally, consequent to the lateral motion of the bubble, the liquid flow distribution around the Taylor bubble tail would become non-uniform and the bubble's wake could become axially asymmetric, creating a lower pressure field in the region below the thicker liquid film. The free surface of the bubble tail could then respond by changing its slope as sketched in Fig. 17, from (a) to (b). Because of asymmetric pressure field below the tail, the Taylor bubble may start moving towards the opposite side of the tube, reaching a new eccentric position. This type of bubble tail movement can be clearly observed in the photographs (Fig. 1) of Kagawa and Kariyasaki (1982),

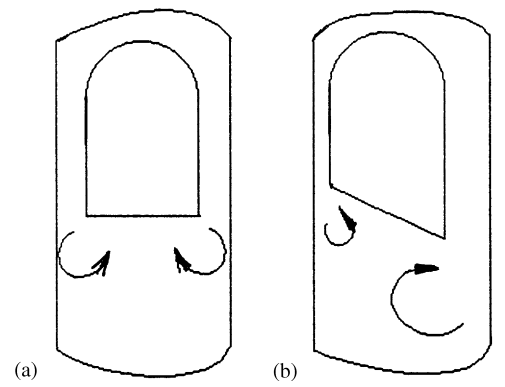

Fig. 17. Different shapes of Taylor bubble tail: (a) at center, (b) off-center.

for consecutive Taylor bubbles in developing slug flow with a cocurrent upward flow of liquid. Furthermore, with the alternating lateral movements of the trailing Taylor bubble from one side of the tube to the other, the instantaneous rise velocity should fluctuate as the trailing Taylor bubble accelerates upward. The instantaneous rise velocities of trailing Taylor bubbles accelerating behind leading Taylor bubbles have been observed to fluctuate in a gas–liquid slug flow (Hasanein et al., 1996), however, the interaction of a Taylor bubble tail with its own wake discussed above should be further investigated.

5. Conclusions

Experiments have been conducted with solid Taylor bubbles suspended in a downward flowing liquid in a vertical tube to determine the drag force variations in single and dual solid Taylor bubble systems, at six different liquid flow rates. All the measurements clearly indicated a significant decrease in the drag force when the bubble was laterally displaced from the tube axis or when the bubble nose is deformed in shape, for both 7.5-cm and 15-cm long bubbles. A one-dimensional model was developed and used to successfully estimate the pressure drop in the liquid and explain the drag force variations with the lateral displacement of the solid Taylor bubble. The drag forces measured for a short (7.5-cm length) solid Taylor bubble with a deformed nose shape were also smaller (by 30%) compared to the values obtained for the bubble of the same length but with an axi-symmetric nose. For the 15-cm length bubbles, the reduction was similarly observed.

The influence of a leading Taylor bubble on a trailing Taylor bubble, both 15-cm long, was clearly seen only at small separation distances (up to $z = 2D$–$3D$). The drag force increased continuously reaching a peak value at $z = 2D$–$3D$, but remained relatively constant at further separation distances. The limited direct influence of the leading bubble's wake was accompanied by nearly the same drag force variations with lateral displacement of the trailing Taylor bubble, at different separation distances ($3D$, $5D$ and $7D$) as in single bubble measurements.

Finally, the similarities and differences between gas–liquid and solid–liquid systems were examined in order to determine the applicability of the present results to gaseous Taylor bubbles in slug flow situations. Although significant differences exist between the two systems, both the lateral displacement and deformation of the gaseous Taylor bubble are expected to reduce the hydraulic resistance for the liquid flowing downward past the bubble and thereby increase the downward liquid flow rate and the gaseous Taylor bubble's rise velocity.

Notation

A_{TB}	Taylor bubble cross-sectional area, m^2
b	blockage ratio
C_1	constant in a friction factor expression
C_c	coefficient of contraction
C_D	drag coefficient
D	tube diameter, m
D_{TB}	Taylor bubble diameter, m
e	bubble eccentricity
$(f_D)_{\text{form}}$	form drag, N
$(f_D)_{\text{skin}}$	friction drag, N
f_D	total drag force, N
f_{sk}	friction factor
g	gravitational acceleration, m/s^2
k	ratio of Taylor bubble to tube diameters
K	total head-loss coefficient
K_{en}	entrance head-loss coefficient
L_{TB}	Taylor bubble length, m
p_1	pressure at the Taylor bubble nose, Pa
p_3	pressure at the Taylor bubble tail, Pa
Q_f	liquid film flow rate, m^3/s
Re	liquid Reynolds number based on mean liquid velocity and tube diameter
Re_f	film Reynolds number based on mean film velocity and hydraulic diameter of an annulus
u	mean liquid velocity in tube, m/s
z	elevation, m

Greek Letters

α	kinetic energy correction factor
δ	liquid film thickness, m
θ	angle in cylindrical coordinates, rad
μ_L	liquid viscosity, kg/ms
ρ_G	gas density, kg/m^3
ρ_L	liquid density, kg/m^3
τ_w	shear stress at the pipe wall, N/m^2
τ_{TB}	shear stress at the bubble surface, N/m^2
ϕ_1	shear stress ratio
Γ_f	volumetric flow rate of liquid film per unit perimeter, m^2/s

Acknowledgements

The authors would like to acknowledge financial support for this work provided by the Natural Sciences and Engineering Research Council of Canada.

References

Ahmad, W. R., DeJesus, J. M., & Kawaji, M. (1998). Falling film hydrodynamics in slug flow. *Chemical Engineering Science*, *53*(1), 123–130.

Akagawa, K., Hamaguchi, H., & Sakaguchi, T. (1966). Fluctuation in void ratio in two-phase flow. *Bulletin of the JSME*, *9*, 104–120.

Batchelor, G. K. (1967). *An introduction to fluid mechanics*. Cambridge: Cambridge University Press.

Bendiksen, K. H. (1984). An experimental investigation of the motion of long bubbles in inclined tubes. *International Journal of Multiphase Flow*, *10*(4), 467–483.

Bendiksen, K. H. (1985). On the motion of long bubbles in vertical tubes. *International Journal Multiphase Flow*, *11*, 797–812.

Bessler, W. F., & Littman, H. (1987). Experimental studies of wakes behind circularly capped bubbles. *Journal of Fluid Mechanics*, *185*, 137–151.

Campos, J. B. L. M., & Geuedes de Carvalho, J. R. F. (1988). An experimental study of the wake of gas slugs rising in liquids. *Journal of Fluid Mechanics*, *196*, 27–37.

Collins, R., DeMoraes, F. F., Davidson, J. F., & Harrison, D. (1978). The motion of a large gas bubble rising through liquid flowing in a tube. *Journal of Fluid Mechanics*, *89*, 497–514.

Couet, B., & Strumolo, G. S. (1987). The effects of surface tension and tube inclination on a two-dimensional rising bubble. *Journal of Fluid Mechanics*, *187*, 1–14.

Davies, R. M., & Taylor, G. I. (1950). The mechanics of large bubbles rising through extended liquids and through liquids in tubes. *Proceedings of the Royal Society of London. Series A*, *200*, 375–390.

DeJesus, J. M., Ahmad, W., & Kawaji, M. (1995). Experimental study of flow structure in vertical slug flow. In *Advances in multiphase flow* (pp. 105–118). Amsterdam: Elsevier.

Dukler, A. E., Maron, D. M., & Brauner, N. (1985). A physical model for predicting minimum stable slug length. *Chemical Engineering Science*, *40*, 1379–1985.

Dumitrescu, D. T. (1943). Stromung an einer Luftblase in Sechrecten Rohr. *Zeitschrift fuer Angewandte Mathematik und Mechanik*, *23*, 139–149.

Fernandes, R. C., Semiat, R., & Dukler, A. E. (1983). Hydrodynamic model for gas-liquid flow in vertical pipes. *A.I.Ch.E Journal*, *29*, 981–989.

Fox, R. W., & McDonald, A. T. (1992). *Introduction to fluid mechanics*. New York: Wiley.

Hanks, R. W. (1963). The laminar-turbulent transition for flow in pipes, concentric annuli, and parallel plates. *A.I.Ch.E. Journal*, *9*, 45–48.

Hasanein, H. A., Tudose, E. T., Wong, S., Malik, M., & Kawaji, M. (1996). Slug flow experiments and computer simulation of slug length distribution in vertical pipes. *A.I.Ch.E. Symposium Series*, *310*(92), 211–219.

Jonsson, V. K., & Sparrow, E. M. (1966). Experiments on turbulent flow phenomena in eccentric annular ducts. *Journal of Fluid Mechanics*, *25*, 65–68.

Kagawa, M., & Kariyasaki, A., (1982). *Visual observation of flow configuration in vertical upward slug flow*. Faculty of Engineering Report, Fukuoka University, Vol. 28, (pp. 139–143).

Karimi, G., & Kawaji, M., (1998). An experimental study of freely falling films in a vertical tube. *Chemical Engineering Science*, *53*(20), 3501–3512.

Liu, H., & Richards, J. L. (1994). Hydraulics of a stationary capsule in pipe. *Journal of Hydraulics Engineering*, *120*(1), 22–40.

Mao, Z. S., & Dukler, A. E. (1989). An experimental study of gas-liquid slug flow. *Experiments in Fluids*, *8*, 169–182.

Mao, Z. S., & Dukler, A. E. (1990). The motion of Taylor bubbles in vertical tubes – I. A numerical simulation for the shape and rise velocity of Taylor bubbles in stagnant and flowing liquid. *Journal of Computational Physics*, *91*, 132–160.

Moissis, R., & Griffith, P. (1962). Entrance effects in two-phase slug flow. *Journal of Heat Transfer*, *84*, 29–39.

Nickens, H. V., & Yannitell, D. W. (1987). The effect of surface tension and viscosity on the rise velocity of a large gas bubble in a closed, vertical liquid-filled tube. *International Journal of Multiphase Flow*, *13*, 57–69.

Nicklin, D. J., Wilkes, J. O., & Davidson, J. F. (1962). Two-phase flow in vertical tubes. *Transactions of the Institution of Chemical Engineers*, *40*, 61–68.

Nusselt, W. (1916). Die Oberflaechen Kondensateion des Wasserdampfes. *VDI Zeitschrift*, *60*, 541–546.

Reinelt, D. A. (1987). The rate at which a long bubble rises in a vertical tube. *Journal of Fluid Mechanics*, *175*, 557–565.

Shemer, L., & Barnea, D. (1987). Visualization of the instantaneous velocity profiles in gas–liquid slug flow. *Phys. Chem. Hydr.*, *8*(3), 243–253.

Street, J. R., & Tek, M. R. (1965). Dynamics of bullet shaped bubbles encountered in vertical gas liquid slug flow. *A.I.Ch.E. Journal*, *11*, 644–650.

Streeter, V. L. (1961). *Handbook of fluid dynamics*. New York: McGraw-Hill Company.

Tiedt, W. (1967). Berechnung des Laminaren and Turbulenten Reibungswiderstandes Konzentrischer und Exzentrischer Ringspalte. *Part II. Chemiker-Zeitung Chemische Apparatus*, *91*, 17–25.

Tudose, E.T., (1997). *Experimental investigation of Taylor bubble acceleration mechanism in slug flow*. M.A.Sc. Thesis, Dept. of Chemical Engineering and Applied Chemistry, University of Toronto.

Zukoski, E. E. (1966). Influence of viscosity, surface tension and inclination angle on motion of long bubbles in closed tubes. *Journal of Fluid Mechanics*, *25*, 821–837.